Reservoir-induced stabilization of a periodically driven classical spin chain: Local versus global relaxation

Thomas Veness and Kay Brandner

School of Physics and Astronomy and Centre for the Mathematics and Theoretical Physics of Quantum Non-equilibrium Systems, University of Nottingham, Nottingham NG7 2RD, United Kingdom

Floquet theory is an indispensable tool for analyzing periodically driven quantum many-body systems. Although it does not universally extend to classical systems, some of its methodologies can be adopted in the presence of well-separated timescales. Here we use these tools to investigate the stroboscopic behaviors of a classical spin chain that is driven by a periodic magnetic field and coupled to a thermal reservoir. We detail and expand our previous work: we investigate the significance of higher-order corrections to the classical Floquet-Magnus expansion in both the high- and low-frequency regimes; explicitly probe the evolution dynamics of the reservoir; and further explore how the driven system and the reservoir synchronize with the applied field at low frequencies. In line with our earlier results, we find that the high-frequency regime is characterized by a local Floquet-Gibbs ensemble with the reservoir acting as a nearly-reversible heat sink. At low frequencies, the driven system rapidly enters a synchronized state, which can only be fully described in a global picture accounting for the concurrent relaxation of the reservoir in a fictitious magnetic field arising from the drive. We highlight how the evolving nature of the reservoir may still be incorporated in a local picture by introducing an effective temperature. Finally, we show that generic local-dissipation models that account for the influence of the reservoir on the driven system phenomenologically through Markovian dissipative equations of motion can generally not reproduce the rich behavior that our microscopic simulations reveal. In particular, such models prove insufficient to account for the suppression of overall energy absorption that is induced by the here observed synchronization between driven system and reservoir.

I. INTRODUCTION

Floquet's theorem states that any homogeneous system of linear differential equations with time-periodic coefficients can be mapped to an autonomous system by means of a linear basis transformation [1]. This transformation carries the same periodicity as the original system and can be chosen to become the identity at integer multiples of the period. When applied to the Schrödinger equation this theorem implies that any periodically driven quantum system is connected by a time-periodic unitary transformation to an undriven system whose dynamics is stroboscopically equivalent [2–6]. Classical equations of motion, however, are generally nonlinear and there is indeed no intuitive counterpart to Floquet's theorem in Hamiltonian mechanics, as can be seen from the following argument [7]. Any autonomous classical system with one degree of freedom is integrable as energy provides the required conserved quantity. By extension, if it were always possible to find a time-periodic canonical transformation that renders its Hamiltonian time independent, any periodically driven system with one degree of freedom would be integrable. This

hypothesis is easily falsified by a counterexample: Kapitza's pendulum, for instance, is known to be nonintegrable despite having only one degree of freedom [8–10]. This observation seems to leave us with a fundamental gap between quantum and classical mechanics.

Indeed, driven by recent experimental advances [11], studies of periodically driven many-body systems have so far mainly focused on the quantum regime, where Floquet theory has exposed a rich landscape of phenomena including sharp notions of nonequilibrium phases with no static counterpart [12,13], new perspectives on many-body quantum chaos [14], and the possibility of engineering specific band structures through precisely tunable driving fields [15,16]. Still, although there is no "classical Floquet theorem," much of the methodology used to describe periodically driven quantum systems, such as the Floquet-Magnus expansion, formally extends to Hamiltonian systems. It is therefore not *a priori* obvious what phenomenology is particular to the quantum realm. In fact, quantum and classical many-body systems are alike in that they generically tend to absorb energy from a periodic drive until they approach a trivial "infinite-temperature ensemble" [17–20]. Some routes to avoid this overheating, such as preventing thermalization through many-body localization [13], draw on quantum effects. Others, like conservation laws [21], may cause observables to synchronize thus giving rise to Gibbs ensembles with time-periodic Lagrange multipliers [22], or the high-frequency limit, where
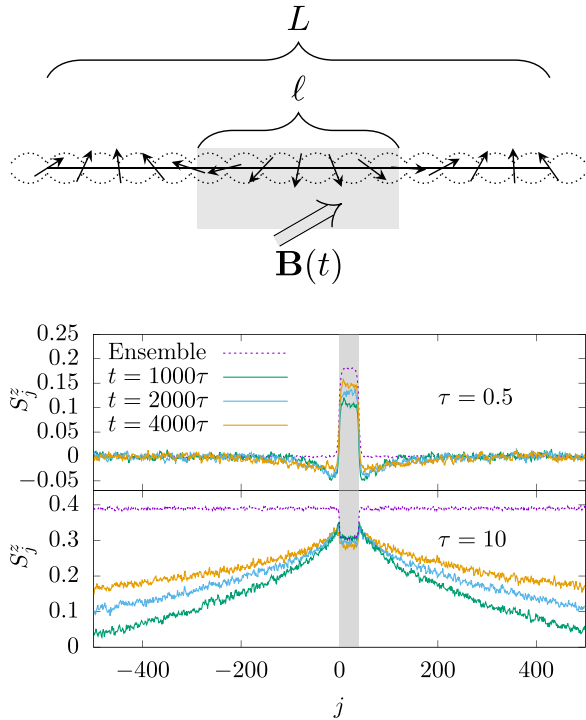
FIG. 1. Top: System. A chain of L classical spins, l of which are subject to a uniform periodic magnetic field $\mathbf{B}(t) = \mathbf{B}(t + \tau)$. All spins have nearly isotropic nearest-neighbor interactions, with small disorder breaking conservation laws. Bottom: Emerging states. The plots show a comparison between dynamical evolutions of the system over the time t and predicted equilibrium expectation values of spatially resolved z magnetization. After a transient phase, both regimes may be described by effective Gibbs ensembles sampled via Monte Carlo techniques. For high frequencies, e.g., $\tau = 0.5$, the driven sites (shaded region) locally see significant evolution. The reservoir, initialized in a thermal state with zero magnetization, remains unchanged up to noise beyond a small correlation length. In contrast, the low-frequency profile, e.g., $\tau = 10$, continues to spread deep into the reservoir at late times, indicating the global nature of the emerging steady state. We have set the parameters $L = 2000$, $\ell = 40$, $e_{\text{initial}} = -0.66$, and $\delta J = 10^{-3}$ and averaged over $\mathcal{N} = 8000$ initial states and disorder realizations (see Sec. II for details).

heating rates are typically exponentially suppressed in the driving frequency [23–27], should, however, be equally accessible in the classical regime. This paper represents a contribution to a growing literature oriented around exploring the phenomenology of classical many-body systems [28–31]. We aim to shed light on the so far relatively unexplored class of classical periodically driven many-body systems, which is potentially ripe with interesting physics. Furthermore, we set out to investigate how the dynamics of such a system can be stabilized away from the high-frequency limit by coupling to a large thermal reservoir.

To these ends, we consider a classical spin chain with nearest-neighbor interactions and weak disorder. A small fraction of this chain, to which we refer as the "system proper," is subject to a rotating magnetic field, with the remainder acting as a "reservoir" (see Fig. 1). Expanding on our previous

work [32], we simulate the full dynamics of this system and compare its emergent steady states with those predicted by Gibbs ensembles. This analysis yields three major insights, which are exposed by the plots of Fig. 1.

First, in the high-frequency regime, the system proper dissipatively relaxes to a stroboscopic Gibbs ensemble at the initial temperature of the reservoir, as if being locally quenched to a new Hamiltonian. During this process, the reservoir absorbs residual heat while nearly remaining in its initial equilibrium state. It thus plays the role of a passive heat sink. The new Hamiltonian of the system proper can be accurately determined by the lowest orders of the classical Floquet-Magnus expansion, which is essentially a systematic method to average over the periodic driving, order by order in the inverse frequency.

Second, even at low and intermediate frequencies, the system proper quickly attains a stroboscopic steady state, which survives well beyond initial transient behavior and is only slowly destabilized by residual heating. Since, in contrast to the high-frequency regime, the driven spins can now follow the applied magnetic field, this state is characterized by synchronization between the drive and the system proper, which leads to a drop in its energy density. At the same time, the state of the reservoir is altered qualitatively as an emerging magnetization profile spreads out from the driven sites and eventually covers the entire spin chain. This effect corresponds to a second stage of synchronization, now between system proper and reservoir, and enables the redistribution of energy over large spatial distances. From the perspective of statistical mechanics, it can be understood as a relaxation process in a rotating reference frame, where the full system approaches a new Gibbs state. The corresponding effective Hamiltonian differs from the original one in both the driven and the undriven parts of the chain. As a result, the effective temperature of the new Gibbs ensemble can deviate substantially from the initial temperature of the reservoir. Notably, this mechanism leads to a strong suppression of the overall energy absorption compared with generic local-dissipation models that rest on the assumption that the reservoir remains constantly in its original equilibrium state.

Third, despite being fundamentally different in nature, the low- and the high-frequency regime are separated only by narrow crossover on the inverse frequency axis. The onset of this transition is predominantly determined by the strength of the interaction between neighboring spins and features a rapid increase in energy absorption. As the driving frequency decreases beyond the crossover, the energy density of the system proper falls off monotonically, while its stroboscopic steady state smoothly approaches the instantaneous Gibbs state that is determined by the original Hamiltonian and the initial temperature of the reservoir.

Our analysis of this phenomenology proceeds as follows. In Sec. II we define the system and outline the numerical techniques for both dynamical simulation, and for statistical sampling of known distributions. In Sec. III we validate these numerical procedures for the undriven system, where we already have a firm theoretical footing in the standard results of statistical mechanics. Here, we set the scene for the main quantities of interest. In Sec. IV we turn towards our main program: investigating the periodically driven dynamics of

a classical many-body system. We approximately construct ensemble descriptions at both high and low frequencies, going beyond the leading order analysis of Ref. [32]. We demonstrate that further corrections are indeed small and consistent with observed data. In Sec. V we investigate the behavior of the reservoir itself and further examine the two stages of synchronization that characterize the low-frequency regime. We further work out an explicit comparison with a generic local-dissipation model, where the reservoir is described effectively through stochastic and dissipative corrections to the equations of motion of the system proper. In Sec. VI, we discuss the broader implications of our results along with perspectives for future research.

II. SYSTEM AND SIMULATION

A. Dynamics

The system under consideration, sketched in Fig. 1, comprises a chain of L three-component classical spins $\mathbf{S}_j$ normalized such that $|\mathbf{S}_j| = 1$. Its Hamiltonian is given by

$$\mathcal{H}(t) = -\sum_{j=1}^{L} \mathbf{S}_j^\top J_j \mathbf{S}_{j+1} + \sum_{j=1}^{\ell} \mathbf{B}(t) \cdot \mathbf{S}_j, \quad (1)$$

where we assume periodic boundary conditions $\mathbf{S}_{L+1} = \mathbf{S}_1$. The rotating magnetic field $\mathbf{B}(t) = (\cos(\omega t), \sin(\omega t), 0)^\top$, with period $\tau = 2\pi/\omega$, acts on the sites $j = 1, \ldots, \ell$, to which we refer as the *system proper*. Accordingly, we call the undriven $L - \ell$ sites the *reservoir*. The coupling matrices are diagonal, $J_j = \text{diag}[J_j^x, J_j^y, J_j^z]$. To break any exact conservation laws constraining the dynamics [33], we choose the J_j^α independently and identically distributed from a normal distribution, with mean J which we set equal to 1 throughout, and variance δJ i.e., $J_j^\alpha \sim \mathcal{N}(1, \delta J)$. To match the dimensions of energies and frequencies, we formally set the reduced Planck constant $\hbar$ equal to 1, hence the spins being dimensionless. The equations of motion are determined by the Poisson bracket $\{S_j^\alpha, S_k^\beta\} = \delta_{jk} \varepsilon^{\alpha\beta\gamma} S_j^\gamma$ via Hamilton's equations

$$\frac{d\mathbf{S}_j}{dt} = -\{\mathcal{H}(t), \mathbf{S}_j\}. \quad (2)$$

This rule yields a coupled system of nonlinear differential equations for the spin degrees of freedom,

$$\frac{d\mathbf{S}_j}{dt} = -\mathbf{\Omega}_j \times \mathbf{S}_j,$$

$$\mathbf{\Omega}_j = J_{j-1}\mathbf{S}_{j-1} + J_j \mathbf{S}_{j+1} - \begin{cases} \mathbf{B}(t), & 1 \leqslant j \leqslant \ell \\ 0 & \text{otherwise.} \end{cases} \quad (3)$$

If the applied field $\mathbf{B}$ were to vanish and all J_j were the identity matrix, the total magnetization $\mathcal{M} = \frac{1}{L} \sum_{j=1}^{L} \mathbf{S}_j$ would be an exactly conserved quantity. To apply the principles of statistical mechanics, we would then have to include these additional conserved quantities through Lagrange multipliers determined by the initial conditions, and any statistical sampling would have to respect this constraint. We add a small amount of Gaussian noise to the couplings J_j to preclude such fine tuning. This disorder breaks all conservation laws, and even in the absence of driving only energy conservation holds,

but does not significantly affect the macroscopic properties of the system otherwise.

To fully determine the dynamics, we now specify the initial conditions for the equations of motion (3). To understand the general behavior of the system, we take a statistical approach rather than focusing on individual trajectories, which may be subject to fluctuations. Our initial states are therefore drawn from a Gibbs ensemble defined by

$$\mathcal{P}_0 = e^{-\beta \mathcal{H}_0}/\mathcal{Z}_0,$$

$$\mathcal{H}_0 = -\sum_{j=1}^{L} \mathbf{S}_j^\top J_j \mathbf{S}_{j+1}, \quad (4)$$

with β being an inverse temperature chosen to fix a specific initial mean energy density, and $\mathcal{Z}_0$ being a normalization constant. With these initial conditions, the system would remain statistically invariant under its time evolution if no magnetic field were applied. Hence, when the field is applied to the system proper, the dynamics of the reservoir are locally in equilibrium and we do not need to account for quenchlike effects. We expect both the slow and fast driving regimes to result in minimal energy absorption, and that the state of the reservoir is only gradually modified. In the following, unless otherwise indicated, all presented results correspond to averages over both initial conditions and realizations of disorder for J_j.

B. Numerical techniques

As given by Eqs. (3), the instantaneous evolution of each spin $\mathbf{S}_j$ is a rotation in an effective magnetic field determined by the on-site magnetic field and the field from its nearest neighbors $\mathbf{S}_{j-1}$ and $\mathbf{S}_{j+1}$. The dynamics of the spin chain may therefore be efficiently simulated using alternated updating [34]. The basic idea of this approach is to split the spin chain into two interleaving subchains A and B comprising the even and odd sites, respectively. The local field for each spin in A depends only on those in B, and vice versa, and we can update these fields alternately. More precisely, the technique we implement is drawn from Refs. [34,35] and uses the simplest Suzuki-Trotter decomposition of the time-evolution operator from time t to $t + \delta t$, $U(t + \delta t, t)$. That is, we have

$$U(t + \delta t, t) = e^{\frac{\delta t}{2} \mathcal{L}_{t+\delta t/2}^A} e^{\delta t \mathcal{L}_{t+\delta t/2}^B} e^{\frac{\delta t}{2} \mathcal{L}_{t+\delta t/2}^A} + \mathcal{O}(\delta t^3). \quad (5)$$

The Liouville operator $\mathcal{L}_{t+\delta t/2}^{A/B}$ generates rotations on the subchain A or B in the effective field determined from subchain B or A at time $t + \delta t/2$. The error of this decomposition is bounded by terms of order δt^3. As the propagation over a time step δt is now formulated solely in terms of rotations, the spin normalization is manifestly preserved by this procedure.

We will make extensive use of Monte Carlo (MC) techniques to sample from particular Gibbs distributions. We use standard Metropolis-Hastings sampling, where a site is chosen randomly with equal probability, and a proposed update of the spin at the particular site pointing in a new direction chosen uniformly from the surface of the unit sphere. The proposed update is then accepted if the energy of the new configuration decreases, i.e., $\Delta E \leqslant 0$, or accepted with probability $e^{-\beta \Delta E}$ if $\Delta E > 0$. As the number of proposals accepted or rejected

increases, this procedure is asymptotically guaranteed to sample from the Gibbs ensemble [36].

III. UNDRIVEN SYSTEM

To set the stage for our main investigations and to confirm the validity of our numerical approach, we first consider the undriven system, reproducing results from Ref. [34]. That is, we set $\mathbf{B} = 0$ so that the Hamiltonian of the entire spin chain is given by $\mathcal{H}_0$ of Eq. (4). We initialize the entire spin chain in a random state with a fixed mean energy and zero total magnetization, which then evolves under the equations of motion (3). The fundamental postulate of statistical mechanics asserts that time averages and ensemble averages are equivalent in an ergodic system. This equivalence extends to all moments of observables, and therefore their full distributions. In a canonical ensemble with inverse temperature β the probability distribution of any observable $\hat{O} = \hat{O}(\{\mathbf{S}_j\})$ reads

$$P_{\text{can}}(O) = \frac{1}{\mathcal{Z}_0} \int d\mathbf{S}_1 \cdots d\mathbf{S}_L e^{-\beta \mathcal{H}_0} \delta[O - \hat{O}(\{\mathbf{S}_j\})], \quad (6)$$

with $\mathcal{Z}_0$ being a normalization, which sums the probability of all configurations compatible with $\hat{O} = O$. Note that we use the canonical ensemble as a matter of convenience throughout. This approach should be equivalent to a microcanonical one up to finite-size corrections.

To confirm that the undriven spin chain satisfies ergodicity, we compute the full probability distributions of macroscopic observables over a *single* trajectory and compare them with the corresponding ensemble distribution (6). For an arbitrary observable $\hat{O}$, we may sample at times $t_1, \ldots, t_\mathcal{N}$, and write the binned probability density with bin width ϵ as

$$P_T(O) = \frac{1}{\mathcal{N}} \sum_{n=1}^{\mathcal{N}} \Pi_\epsilon[O - \hat{O}(\{\mathbf{S}_j(t_n)\})], \quad (7)$$

where the sample times are given by $t_n = t_0 + n\Delta t$, choosing t_0, Δt, and $\mathcal{N}$ sufficiently large such that the result is insensitive to specific values. The function Π_ϵ counts the number of points along the trajectory, where the value of $\hat{O}$ lies within the window of width ϵ centered at O. In other words, Π_ϵ is an approximation of a delta function, formally given by

$$\Pi_\epsilon[x] = \frac{1}{\epsilon} \begin{cases} 1, & -\epsilon/2 \leqslant x \leqslant \epsilon/2 \\ 0 & \text{otherwise.} \end{cases} \quad (8)$$

MC sampling is a numerical technique that generates samples in the correct proportions as determined by a given probability distribution, without having to exhaustively explore the phase space of the system. We may therefore construct the ensemble distribution (6) for any observable by using M MC samples as outlined in Sec. II B. Specifically, the equivalent of Eq. (7) for the Gibbs ensemble is

$$P_{\text{can}}(O) = \frac{1}{M} \sum_{m=1}^{M} \Pi_\epsilon[O - \hat{O}(\{\mathbf{S}_j^{(m)}\})], \quad (9)$$

where $\mathbf{S}_j^{(m)}$ is the mth MC sample. We note that the MC algorithm samples from the canonical ensemble, and due to energy conservation the dynamical trajectory is sampling from the microcanonical ensemble. However, when comparing local

observables involving only degrees of freedom of the first $\ell \ll L$ sites, even the energy density will fluctuate, and the equivalence of ensembles implies that all results should be identical up to finite-size effects.

In Fig. 2, we show that single-trajectory and ensemble distributions are in excellent agreement for the representative observables

$$\mathbf{m} = \frac{1}{\ell} \sum_{j=1}^{\ell} \mathbf{S}_j,$$

$$e = -\frac{1}{\ell - 1} \sum_{j=1}^{\ell-1} \mathbf{S}_j^\top J_j \mathbf{S}_{j+1}, \quad (10)$$

i.e., the magnetization and energy density of the system proper. This result confirms that the undriven system behaves ergodically even if $\delta J = 10^{-3}$ is small. For the isotropic chain, $\delta J = 0$, we may also compute the exact probability distribution for the energy density at large ℓ. We here consider open boundary conditions, which are equivalent to periodic boundary conditions up to finite-size corrections. First, the partition function is given by

$$Z = \int d\mathbf{S}_1 \cdots d\mathbf{S}_\ell \, e^{\beta \sum_{j=1}^{\ell-1} \mathbf{S}_j \cdot \mathbf{S}_{j+1}}, \quad (11)$$

where $d\mathbf{S}_j = \frac{1}{4\pi} \sin \theta_j d\theta_j d\phi_j$ indicates integration over the spherical angles of each spin. Rewriting this expression in terms of the angle between adjacent spins in the chain, we find

$$Z = \left[\frac{1}{2} \int_{-1}^{1} d\cos\theta \, e^{\beta \cos\theta} \right]^{\ell-1} = \left(\frac{\sinh\beta}{\beta} \right)^{\ell-1}. \quad (12)$$

Hence, the free energy density of the isotropic chain at inverse temperature β is given by [37]

$$f(\beta) = -\frac{1}{\beta(\ell - 1)} \ln Z = -\frac{1}{\beta} \ln \frac{\sinh\beta}{\beta}. \quad (13)$$

We may thus calculate the probability distribution for the energy density e of Eq. (10) as

$$P(e) = \frac{1}{Z} \int d\mathbf{S}_1 \cdots d\mathbf{S}_\ell \, e^{\beta \sum_{j=1}^{\ell-1} \mathbf{S}_j \cdot \mathbf{S}_{j+1}}$$

$$\times \int_{-\infty}^{\infty} \frac{dz}{2\pi} e^{iz(e(\ell-1) + \sum_{j=1}^{\ell-1} \mathbf{S}_j \cdot \mathbf{S}_{j+1})}, \quad (14)$$

where we have used the Fourier representation of the Dirac delta function appearing in Eq. (6). Employing the method of steepest descent [38], this integral may be approximated as

$$P_\ell(e) = \frac{\mathcal{Q}}{\sqrt{(\ell - 1)|g''(z^*)|}} e^{-(\ell-1)g(z^*)}, \quad (15)$$

where $\mathcal{Q}$ is a normalization constant, and β is chosen to fix the mean energy density $\frac{1}{\beta} - \coth\beta = \langle e \rangle$. The function $g(z) = (\beta - z)f(\beta - z) + ez$ determines the saddle point, which is given by z^* such that $g'(z^*) = 0$. Figure 2(a) shows that the exact distribution (15) agrees well with both numerical approaches. This result confirms weak disorder $\delta J \ll 1$ eliminates conservation laws but has no visible effect on the distributions of macroscopic observables.
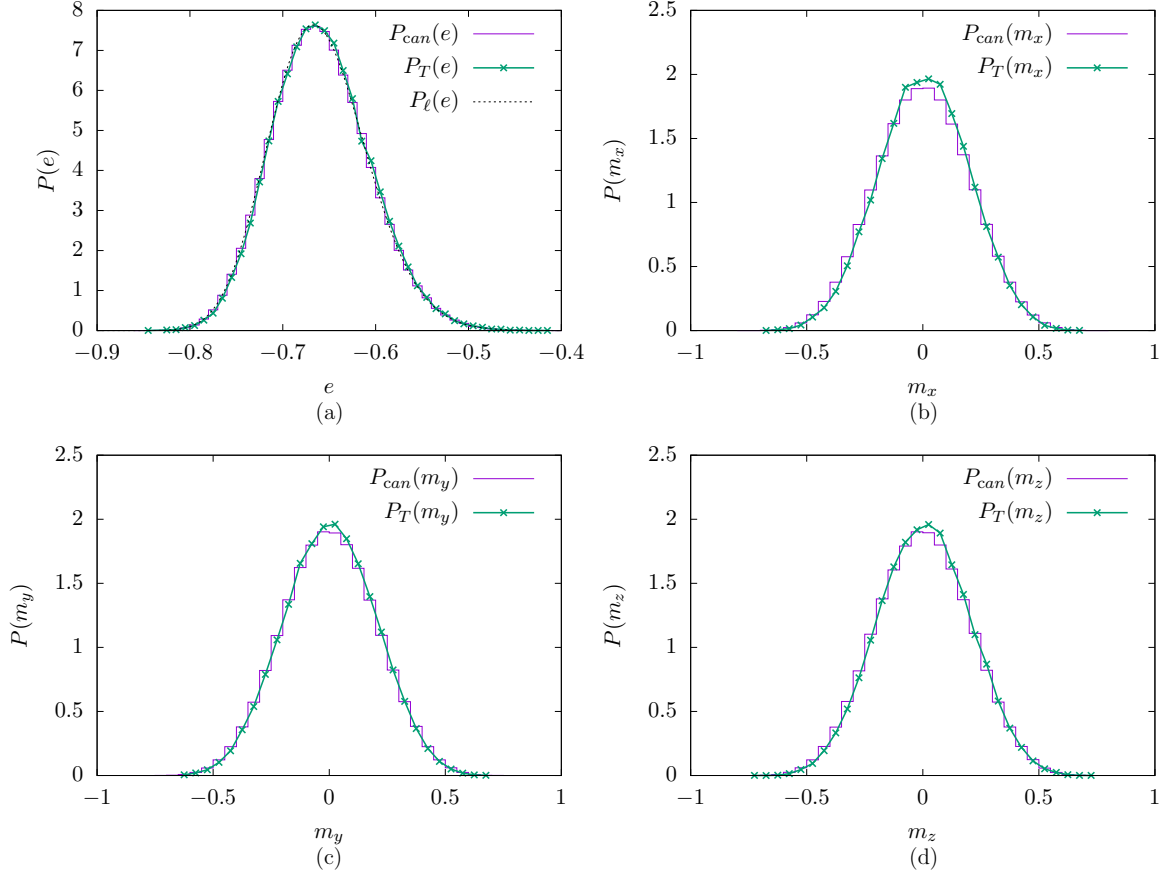
FIG. 2. Undriven system. Histograms showing $P_T(O)$ of Eq. (7) determined from one trajectory with $\mathcal{N} = 64\,000$ samples (crosses), compared with $P_{\text{can}}(O)$ of Eq. (9), where each Monte Carlo curve is binned from $M = 64\,000$ samples. The shown observables are (a) energy density, (b) x magnetization, (c) y magnetization, and (d) z magnetization. For all plots, we have set $L = 2000$, $\ell = 40$, and $\delta J = 2 \times 10^{-3}$, and chosen the energy density of the entire system $e_{\text{initial}} = -0.66$, which implicitly fixes the inverse temperature β for the MC simulation. The exact result (dashed line) of Eq. (15) is also shown in (a).

IV. DRIVEN SYSTEM

Having established that the undriven system is ergodic, we now turn to the effect of periodic driving. Our basic expectations are as follows: at high frequencies, the driving "averages out" and the dynamics are described by the Hamiltonian with no applied field $\mathcal{H}_0$ of Eq. (4); at very low frequencies, the system relaxes to its instantaneous Gibbs state. Here, we develop these expectations into quantitative descriptions of the two regimes, which we show to predict the behavior of the system over a remarkably wide range of frequencies [32]. We note that, for the driven system, we use the definition

$$e = -\frac{1}{\ell - 1} \sum_{j=1}^{\ell} \mathbf{S}_j^\top J_j \mathbf{S}_{j+1} + \frac{1}{\ell} \sum_{j=1}^{\ell} \mathbf{B}(t) \cdot \mathbf{S}_j \quad (16)$$

for the energy density of the system proper, while the magnetization density is still defined as in Eq. (10).

A. High frequency

Intuitively, the physics at high frequencies should be well approximated by the averaged Hamiltonian. This intuition is captured by the Floquet-Magnus expansion. This technique proceeds by assuming that a time-independent generator for the stroboscopic dynamics does exist, and then constructs it order by order in the driving period [39]. The Floquet-Magnus expansion was originally devised for linear systems, and is expansively used for the description of periodically driven quantum systems. It can, however, be adapted to classical Hamiltonian systems, whose dynamics are nonlinear, by formally treating the Poisson bracket as a linear operator. That is, we write the equations of motion for a phase-space observable of the isolated system proper, $\hat{O}(\mathbf{S}_1, \ldots, \mathbf{S}_\ell)$, in the form

$$\frac{d\hat{O}(t)}{dt} = \mathcal{L}_{H(t)} \hat{O}(t), \quad (17)$$

where $\mathcal{L}_{H(t)} \cdot = -\{H(t), \cdot\}$ denotes the Liouville operator and

$$H(t) = -\sum_{j=1}^{\ell-1} \mathbf{S}_j^\top J_j \mathbf{S}_{j+1} + \sum_{j=1}^{\ell} \mathbf{B}(t) \cdot \mathbf{S}_j \quad (18)$$

is the Hamiltonian of the driven system proper. If the Floquet theorem were to hold, the formal solution of Eq. (17) at $t = n\tau$ would take the form

$$\hat{O}(n\tau) = e^{n\tau \mathcal{L}_{H_F}} \hat{O}(0), \quad (19)$$

where H_F would be the Floquet Hamiltonian. While such an object does not exist in general, it can still be perturbative

constructed close to the infinite frequency limit $\tau \to 0$, where $H_F \to \frac{1}{\tau} \int_0^\tau dt H(t)$. To this end, we introduce the dimensionless time $s = t/\tau$ and make the ansatz

$$\hat{O}'(s) = \hat{O}(s\tau) = e^{\mathcal{L}_{K(s)}} \hat{O}'(s), \tag{20}$$

with $0 \leqslant s \leqslant 1$ and the Magnus Hamiltonian

$$K(s) = \sum_{n=0}^{\infty} \tau^n K^{(n)}(s). \tag{21}$$

Upon inserting this ansatz into the equation of motion for $\hat{O}'(s)$ and following the formal steps of the conventional Magnus expansion [2], $K(s)$ can be determined order by order. Returning to original units then yields the effective Floquet Hamiltonian

$$H_F = \frac{1}{\tau} K(t = \tau) = \sum_{n=0}^{\infty} H_F^{(n)}, \tag{22}$$

where the first few terms are given by

$$H_F^{(0)} = \frac{1}{\tau} \int_0^\tau dt \, H(t),$$

$$H_F^{(1)} = \frac{1}{2!\tau} \int_0^\tau dt_1 \int_0^{t_1} dt_2 \, \{H(t_1), H(t_2)\},$$

$$H_F^{(2)} = \frac{1}{3!\tau} \int_0^\tau dt_1 \int_0^{t_1} dt_2 \int_0^{t_2} dt_3$$
$$\times \{H(t_1), \{H(t_2), H(t_3)\}\}$$
$$+ \{H(t_3), \{H(t_2), H(t_1)\}\}. \tag{23}$$

This expansion can in general only be expected to be asymptotic [40–42], and one usually truncates the sum in Eq. (22) after the first few terms. Evaluating the first two expressions explicitly, we find

$$H_F^{(0)} = -\sum_{j=1}^{L} \mathbf{S}_j^\top J_j \mathbf{S}_{j+1},$$

$$H_F^{(1)} = -\frac{1}{\omega} \sum_{j=1}^{\ell}{}' \left(\frac{1}{2} S_j^z + \hat{\mathbf{y}} \cdot (\mathbf{\Omega}_j \times \mathbf{S}_j) \right), \tag{24}$$

where we have introduced the notation $\sum_{j=1}^{\ell}{}'$ meaning that summation is restricted to terms only including spins living on sites $1, \ldots, \ell$, with all other terms being set to zero. Noting that $H_F^{(0)}$ is equal to the Hamiltonian of the initial ensemble in Eq. (4), we must consider at least the first order in τ of the Floquet-Magnus expansion to observe deviations from the initial state. In our previous work the corrections from $H_F^{(1)}$ were observable and consistent with the true dynamics for $\tau \lesssim 1$ [32].

In general, we may write

$$H_F^{(n)} = h_{SB}^{(n)} + h_{MB}^{(n)}, \tag{25}$$

where $h_{SB}^{(n)}$ accounts for single-body terms, and $h_{MB}^{(n)}$ accounts for many-body terms. Accordingly,

$$h_{SB}^{(1)} = -\frac{1}{2\omega} \sum_{j=1}^{\ell}{}' \frac{1}{2} S_j^z, \tag{26}$$

$$h_{MB}^{(1)} = -\frac{\hat{\mathbf{y}}}{\omega} \cdot \sum_{j=1}^{\ell}{}' \mathbf{\Omega}_j \times \mathbf{S}_j, \tag{26}$$

where again sums are restricted to terms only involving spins on the sites $1, \ldots, \ell$. It is interesting to ask if including higher-order corrections from $H_F^{(2)}$ improves the results of Ref. [32] further. Calculating $H_F^{(2)} = h_{SB}^{(2)} + h_{MB}^{(2)}$ yields

$$h_{SB}^{(2)} = \frac{1}{2\omega^2} \sum_{j=1}^{\ell}{}' S_j^x,$$

$$h_{MB}^{(2)} = \frac{1}{2\omega^2} \sum_{j=1}^{\ell}{}' \Bigg\{ 2\hat{\mathbf{x}} \cdot [\mathbf{\Omega}_j \times (\mathbf{\Omega}_j \times \mathbf{S}_j)$$
$$+ (J_{j-1}(\mathbf{\Omega}_{j-1} \times \mathbf{S}_{j-1}) + J_j(\mathbf{\Omega}_{j+1} \times \mathbf{S}_{j+1})) \times \mathbf{S}_j]$$
$$+ \frac{1}{2} \big(3\Omega_j^x S_j^x + \Omega_j^y S_j^y - J_{j-1}^y S_j^z S_{j-1}^z$$
$$- J_j^y S_j^z S_{j+1}^z - J_{j-1}^z S_j^y S_{j-1}^y - J_j^z S_j^y S_{j+1}^y$$
$$- 3J_{j-1}^x S_j^z S_{j-1}^z - 3J_j^x S_j^z S_{j+1}^z$$
$$- 3J_{j-1}^z S_j^x S_{j-1}^x - 3J_j^z S_j^x S_{j+1}^x \big) \Bigg\}. \tag{27}$$

The single-body terms $h_{SB}^{(n)}$ constitute the Floquet-Magnus expansion under the free Hamiltonian $H_{\text{free}} = \sum_{j=1}^{\ell} \mathbf{B}(t) \cdot \mathbf{S}_j$, a linear system for which the expansion may be resummed to yield the effective field of the rotating frame $\mathbf{B}_{\text{rot}} = \hat{\mathbf{x}} - \omega \hat{\mathbf{z}}$ [43]. The many-body terms have more complex structure and become increasingly nonlocal at each subsequent order.

Assuming that the stroboscopic dynamics of the system proper is asymptotically equivalent to the autonomous dynamics of the associated Floquet system, we may define the Nth-order Floquet-Magnus ensemble by

$$P_F^{(N)} = \frac{1}{Z_F^{(N)}} \exp \left(-\beta \sum_{n=0}^{N} H_F^{(n)} \right), \tag{28}$$

where $Z_F^{(N)}$ accounts for normalization. As we expect absorption to be exponentially small in ω at high frequencies [44], we neglect heating and assume the temperature of the ensemble to be well approximated by that of the initial state defined by Eq. (4). As may be seen in Fig. 3, including additional terms in the Magnus ensemble beyond $N = 1$ produces only minimal improvement on the previously observed results at $\tau = 0.5$. We can thus conclude that the two lowest orders of the Floquet-Magnus expansion are indeed sufficient to describe the stroboscopic steady state of the system proper, even well away from the infinite-frequency limit.

B. Low frequency

1. Leading order

The results of the previous section show that the high-frequency regime can be fully described in a local picture focusing only on the system proper and treating the reservoir as a passive heat sink. To understand the low-frequency regime, we must adopt a global picture, where both system proper and reservoir are affected by the driving. This approach is motivated by the observation that the stroboscopic dynamics of the full system are nearly equivalent to the dynamics of an autonomous Floquet system for sufficiently small δJ but
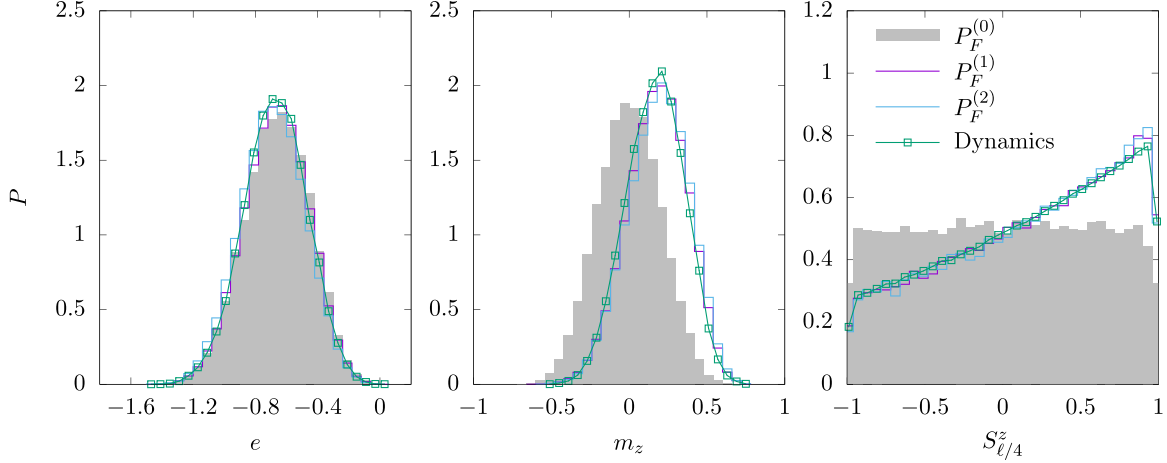
FIG. 3. High-frequency picture. Histogram distributions for $\tau = 0.5$ of the energy density and z magnetization of the system proper, e and m_z, and the z component of the spin at site $f = \ell/4$, $S^z_{\ell/4}$, in the Nth-order Floquet-Magnus ensembles as defined by Eq. (28) for $N = 0, 1, 2$ compared with dynamical evaluations. Statistical ensembles are sampled according to Eq. (9), and the dynamical ones according to Eq. (7) using multiple trajectories and choosing t_0 long enough for observables to relax. For all plots, we have set $L = 2000$, $\ell = 40$, and $\delta J = 0.02$, and chosen the initial energy density $e_{\text{initial}} = -0.66$, which fixes the inverse temperature β for the MC simulation. Due to the minimal energy absorption, we sample multiple points from each trajectory after a transient period to improve statistics. Here we sample 4000 points each from 200 separate trajectories, from the interval $t = 6000\tau$ to $t = 10\,000\tau$. The ensemble histograms were generated from $M = 32\,000, 64\,000$, and $32\,000$ MC samples for $P_F^{(0)}$, $P_F^{(1)}$, and $P_F^{(2)}$, respectively.

arbitrary ω. Specifically, upon introducing the rotating-frame variables

$$\widetilde{\mathbf{S}}_j = \begin{pmatrix} \cos(\omega t) & \sin(\omega t) & 0 \\ -\sin(\omega t) & \cos(\omega t) & 0 \\ 0 & 0 & 1 \end{pmatrix} \mathbf{S}_j, \qquad (29)$$

the equations of motion (3) may be recast as

$$\frac{d\widetilde{\mathbf{S}}_j}{dt} = -\widetilde{\boldsymbol{\Omega}}_j \times \widetilde{\mathbf{S}}_j + \mathcal{O}(\delta J),$$

$$\widetilde{\boldsymbol{\Omega}}_j = \bar{J}_{j-1}\widetilde{\mathbf{S}}_{j-1} + \bar{J}_j\widetilde{\mathbf{S}}_{j+1}$$

$$- \omega\hat{\mathbf{z}} + \begin{cases} \hat{\mathbf{x}}, & 1 \leqslant j \leqslant \ell \\ 0 & \text{otherwise.} \end{cases} \qquad (30)$$

Thus, upon neglecting time-dependent terms of order δJ, the dynamics in the rotating frame are generated by the time-independent Hamiltonian

$$\mathcal{H}_{\text{rot}} = -\sum_{j=1}^{L} \left(\widetilde{\mathbf{S}}_j^\top \bar{J}_j \widetilde{\mathbf{S}}_{j+1} + \omega\hat{\mathbf{z}} \cdot \widetilde{\mathbf{S}}_j\right) + \sum_{j=1}^{\ell} \hat{\mathbf{x}} \cdot \widetilde{\mathbf{S}}_j, \qquad (31)$$

where $\bar{J}_j = \text{diag}[\frac{1}{2}(J_j^x + J_j^y), \frac{1}{2}(J_j^x + J_j^y), J_j^z]$. This result shows that the observable $\mathcal{H}_{\text{rot}}$, which plays the role of a global Floquet Hamiltonian, is nearly conserved in the rotating frame. At the same time $\mathcal{H}_{\text{rot}}$ is a sum of local densities. Hence, by usual arguments of statistical mechanics, the entire system should relax to an ensemble of the form

$$\mathcal{P}_{\text{rot}} = e^{-\beta_{\text{rot}}\mathcal{H}_{\text{rot}}}/\mathcal{Z}_{\text{rot}}. \qquad (32)$$

Note that formally, the system should be described by a microcanonical ensemble. However, for all local observables the canonical ensemble above should provide an equivalent description up to finite-size effects.

The effective inverse temperature β_{rot} may now be determined from the fact that $\mathcal{H}_{\text{rot}}$ is an almost conserved quantity:

assuming that the system has fully relaxed to the ensemble described by Eq. (32), and that persistent heating has only minor effects, the mean value of $\mathcal{H}_{\text{rot}}$ in the initial state $\mathcal{P}_0$ of Eq. (4) should be nearly identical to its mean value in the steady state of Eq. (32). That is, the equation

$$\int d\mathbf{S}_1 \cdots d\mathbf{S}_L \mathcal{H}_{\text{rot}} \mathcal{P}_0 = \int d\mathbf{S}_1 \cdots d\mathbf{S}_L \mathcal{H}_{\text{rot}} \mathcal{P}_{\text{rot}} \qquad (33)$$

implicitly fixes β_{rot} according to standard arguments of statistical mechanics. Upon integrating out the reservoir degrees of freedom in Eq. (32), we thus find the effective stroboscopic ensemble

$$P_{\text{rot}} = \frac{1}{Z_{\text{rot}}} e^{-\beta_{\text{rot}}^{\text{stat}} H_{\text{rot}}}, \qquad (34)$$

where Z_{rot} is a normalization and now the rotating-frame Hamiltonian is, up to δJ corrections and boundary effects,

$$H_{\text{rot}} = -\sum_{j=1}^{\ell-1} \widetilde{\mathbf{S}}_j^\top \bar{J}_j \widetilde{\mathbf{S}}_{j+1} + \sum_{j=1}^{\ell} (\hat{\mathbf{x}} - \omega\hat{\mathbf{z}}) \cdot \widetilde{\mathbf{S}}_j. \qquad (35)$$

As reported in Ref. [32], the ensemble of Eq. (34) yields excellent results for the distribution of system-proper observables at very low frequencies, e.g., $\tau = 10$. In this limit, the effective inverse temperature β_{rot} can be regarded as a property of the reservoir only, since the contributions of the system proper to both averages in Eq. (33) are negligible for $L \gg l$ (see Fig. 4, left panel).

For higher frequencies, however, we find in Fig. 5 that these ensemble distributions deviate significantly from the dynamical ones (see also Fig. 4, right panel). Nonetheless, the ensemble of Eq. (34) reproduces the dynamical full distributions if $\beta_{\text{rot}}^{\text{stat}}$ is replaced with some $\beta_{\text{rot}} = \beta_{\text{rot}}^* < \beta_{\text{rot}}^{\text{stat}}$, which can be found by fitting the mean energy density of the system proper. These discrepancies highlight the limitations of the
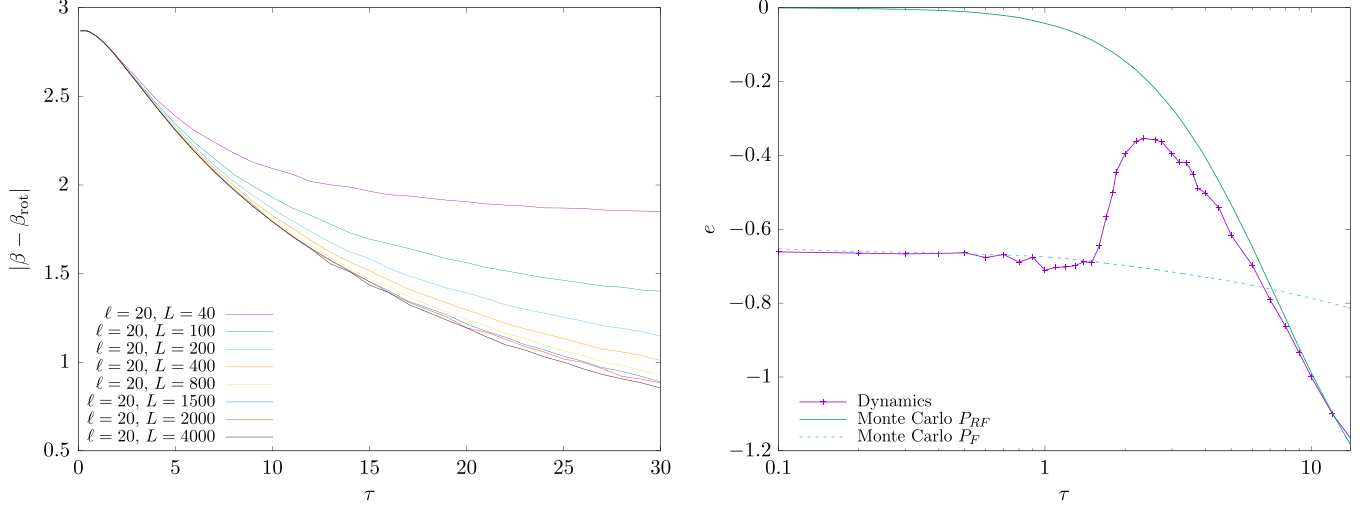
FIG. 4. Effective temperature of the rotating-frame ensemble. Left: The full system is initially prepared in a Gibbs state with respect to its free Hamiltonian $\mathcal{H}_0$ and the inverse temperature $\beta = 2.888$, which corresponds to $\mathfrak{e}_{\text{initial}} = -0.66$. We then determine the effective inverse temperature β_{rot} of the rotating-frame ensemble (32) so that condition (33) is satisfied. The plot has been obtained from $M = 8000$ MC samples with $\delta J = 10^{-3}$, $\ell = 20$, and different values of L. For $L \gtrsim 1500$, the deviation $|\beta - \beta_{\text{rot}}|$ does not change significantly anymore with L, which shows that, in the thermodynamic limit, β_{rot} does not depend on the size and properties of the system proper. Right: Energy density of the system proper as determined from dynamical simulations and the ensembles of Eq. (28) with $N = 1$ (high frequency), and Eq. (34) (low frequency), with β_{rot} determined from Eq. (33). Here, we have set $e_{\text{initial}} = -0.66$, $\ell = 20$, $L = 2000$, $t = 1000\tau$, and $\delta J = 10^{-3}$. The dynamical data correspond to averages over $\mathcal{N} = 8000$ trajectories; the curves for the high- and low-frequency ensembles were obtained from $M = 8000$ MC samples. The first-order Floquet-Magnus ensemble reproduces the energy density of the system proper accurately for $\tau \lesssim 1$, while the rotating-frame ensemble is accurate for $\tau \gtrsim 7$.

assumptions made in writing down Eq. (33), which we explore further in Sec. V. Still, our results indicate that, even close to the crossover into the high-frequency regime, the statistics of the system proper is described by an effective Gibbs state, which depends only on a single fitting parameter.

2. Higher-order corrections

We have so far discarded corrections in δJ, assuming their effects are perturbatively small, but did not yet justify this simplification. In the case of high-frequency driving, the Magnus expansion provides a suitable scheme where corrections are

asymptotically small in τ. This technique can still be applied in the low-frequency regime to obtain systematic corrections to the leading-order picture discussed above. To this end, we observe that the full equations of motion, retaining corrections neglected in Eq. (30), in the rotating frame are given by

$$
\begin{aligned}
\frac{d\widetilde{\mathbf{S}}_j}{dt} = & -(\bar{J}_{j-1}\widetilde{\mathbf{S}}_{j-1} + \bar{J}_j\widetilde{\mathbf{S}}_{j+1}) \times \widetilde{\mathbf{S}}_j \\
& - (\delta J_{j-1}(t)\widetilde{\mathbf{S}}_{j-1} + \delta J_j(t)\widetilde{\mathbf{S}}_{j+1}) \times \widetilde{\mathbf{S}}_j \\
& + \begin{cases} \hat{\mathbf{x}} - \omega\hat{\mathbf{z}}, & \text{if } 1 \leqslant j \leqslant \ell, \\ -\omega\hat{\mathbf{z}}, & \text{if } \ell < j \leqslant L, \end{cases} \times \widetilde{\mathbf{S}}_j,
\end{aligned} \quad (36)
$$
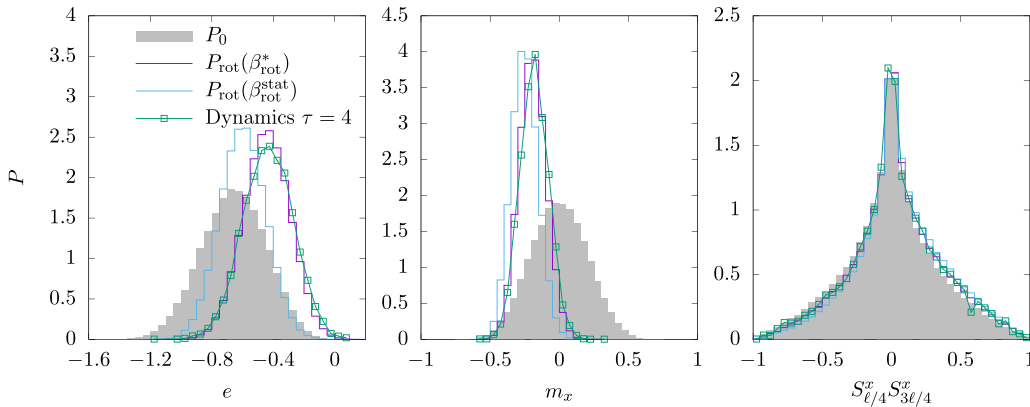
FIG. 5. Low-frequency picture. Histogram distributions for observables of the system proper at $\tau = 4$: comparing $\mathcal{N} = 6000$ dynamical evolutions sampled at $t = 1000\tau$, with $M = 256\,000$ MC samples from ensemble of Eq. (34) for both $\beta_{\text{rot}} = \beta_{\text{rot}}^{\text{stat}}$ and best fit β_{rot}^*. For reference, the initial ensemble P_0 of Eq. (4) is shown in grey. From left to right, the plots show energy density, x-magnetization density, and a two-point spatial correlation function of the x components of the spins at $j = \ell/4$ and $j = 3\ell/4$. Here we have set $\ell = 40$, $L = 4000$, $\delta J = 10^{-3}$, and $e_{\text{initial}} = -0.66$.

where

$$\bar{J}_j = \begin{pmatrix} \frac{1}{2}\left(J_j^x + J_j^y\right) & 0 & 0 \\ 0 & \frac{1}{2}\left(J_j^x + J_j^y\right) & 0 \\ 0 & 0 & J_j^z \end{pmatrix},$$

$$\delta J_j(t) = \frac{\Delta J_j}{2} \begin{pmatrix} -\cos(2\omega t) & \sin(2\omega t) & 0 \\ \sin(2\omega t) & \cos(2\omega t) & 0 \\ 0 & 0 & 0 \end{pmatrix}, \qquad (37)$$

$$\Delta J_j = J_j^y - J_j^x.$$

These equations of motion are generated by the Hamiltonian

$$\mathcal{H}_{\text{rot}}(t) = -\sum_{j=1}^{L} \left[\widetilde{\mathbf{S}}_j^\top (\bar{J}_j + \delta J_j(t)) \widetilde{\mathbf{S}}_{j+1} + \omega \hat{\mathbf{z}} \cdot \widetilde{\mathbf{S}}_j \right]$$
$$+ \sum_{j=1}^{\ell} \hat{\mathbf{x}} \cdot \widetilde{\mathbf{S}}_j. \qquad (38)$$

We see that time-dependent corrections are formally of order δJ. While we are not in the high-frequency regime, we nonetheless have an energy scale parametrically smaller than the driving frequency, $\omega \gg \delta J$. Thus, over the course of one cycle of the drive, we can average over the dynamics induced by the oscillating contributions proportional to δJ. That is, we may employ the Floquet-Magnus expansion in the *rotating* frame, which will generate an asymptotic series in powers of $\delta J/\omega$. After some algebra, we find the first-order global Floquet Hamiltonian in the rotating frame,

$$\mathcal{H}_F^{\text{rot}} = \mathcal{H}_{\text{rot}}^{(0)} + \mathcal{H}_{\text{rot}}^{(1)} + \mathcal{O}(\tau^2),$$

$$\mathcal{H}_{\text{rot}}^{(0)} = -\sum_{j=1}^{L} \left(\widetilde{\mathbf{S}}_j^\top J_j \widetilde{\mathbf{S}}_{j+1} + \omega \hat{\mathbf{z}} \cdot \widetilde{\mathbf{S}}_j \right) + \sum_{j=1}^{\ell} \hat{\mathbf{x}} \cdot \widetilde{\mathbf{S}}_j,$$

$$\mathcal{H}_{\text{rot}}^{(1)} = -\frac{1}{16\omega} \sum_{j=1}^{L} \{ \Delta J_j \Delta J_j (\sigma^z \widetilde{\mathbf{S}}_j) \cdot (\sigma^x \widetilde{\mathbf{S}}_j) \times \widetilde{\mathbf{S}}_{j+1}$$
$$+ \Delta J_{j-1} \Delta J_{j-1} (\sigma^z \widetilde{\mathbf{S}}_j) \cdot (\sigma^x \widetilde{\mathbf{S}}_j) \times \widetilde{\mathbf{S}}_{j-1}$$
$$+ \Delta J_{j-1} \Delta J_j \widetilde{\mathbf{S}}_j \cdot [(\sigma^z \widetilde{\mathbf{S}}_{j+1}) \times (\sigma^x \widetilde{\mathbf{S}}_{j-1})$$
$$- (\sigma^x \widetilde{\mathbf{S}}_{j+1}) \times (\sigma^z \widetilde{\mathbf{S}}_{j-1})] \}, \qquad (39)$$

where we have introduced the matrices

$$\sigma^z = \begin{pmatrix} 1 & 0 & 0 \\ 0 & -1 & 0 \\ 0 & 0 & 0 \end{pmatrix}, \quad \sigma^x = \begin{pmatrix} 0 & 1 & 0 \\ 1 & 0 & 0 \\ 0 & 0 & 0 \end{pmatrix}. \qquad (40)$$

It is natural to ask whether we can distinguish these corrections coming from $\mathcal{H}_{\text{rot}}^{(1)}$ at the level of nonequilibrium ensembles. Upon recalling that $\Delta J_j \sim \delta J$, one would expect the expansion to have a leading contribution with a prefactor $\delta J/\omega$, which we would expect to be distinguishable in distributions of observables. For the specific drive considered, however, we see from Eq. (39) that these corrections vanish and the leading terms are in fact of order $(\delta J)^2/\omega$. Hence, for any practically relevant frequency regime, higher-order corrections may be safely neglected.

V. NATURE AND ROLE OF THE RESERVOIR

Here we expand on the role that the reservoir plays in stabilizing the stroboscopic nonequilibrium steady states constructed in Sec. IV. We first demonstrate how finite disorder rapidly causes runaway heating in the bare driven system away from high frequencies. Coupling a reservoir establishes a channel for heat transport away from the driven sites. Thus, at high frequencies, residual heating is compensated by dissipation with the reservoir acting as a nearly-reversible heat sink. At low frequencies, however, the system proper and the reservoir synchronize with the drive on different timescales. This effect suppresses the net heat uptake of the entire spin chain and stabilizes a nontrivial steady state of the system proper at low and intermediate frequencies. To corroborate this picture, we evaluate spatially resolved observables and explore the inhomogeneous distribution of magnetization within the reservoir. To demonstrate the non-Markovian nature of the reservoir and its role in suppressing energy absorption in the low-frequency regime, we compare our results with those obtained for a generic local-dissipation model in which the reservoir is described phenomenologically through dissipative corrections to the equations of motion of the system proper.

A. High-frequency regime

To understand how the reservoir modifies the dynamics, we calculate the mean energy absorption of the driven system proper with and without a reservoir. The results of this analysis, which are shown in Fig. 6, suggest that the high-frequency regime is "universal" in that the leading-order Magnus physics is insensitive to both weak disorder δJ and the presence of a reservoir. This behavior can be intuitively understood from the structure of the Floquet-Magnus expansion discussed in Sec. IV. To this end, we may divide the Hamiltonian of the entire spin chain into system-proper and reservoir contributions:

$$\mathcal{H}(t) = H^S(t) + H^R,$$

$$H^S(t) = -\sum_{j=1}^{\ell-1} \mathbf{S}_j^\top J_j \mathbf{S}_{j+1} + \sum_{j=1}^{\ell} \mathbf{B}(t) \cdot \mathbf{S}_j, \qquad (41)$$

$$H^R = -\sum_{j=\ell}^{L} \mathbf{S}_j^\top J_j \mathbf{S}_{j+1}.$$

The two lowest-order terms of the Floquet-Magnus expansion are then given by

$$\mathcal{H}_F^{(0)} = \frac{1}{\tau} \int_0^\tau \mathrm{d}t \, \mathcal{H}(t) = \mathcal{H}_0,$$

$$\mathcal{H}_F^{(1)} = h_{F,\,\text{loc}}^{(1)} + h_{F,\,\text{int}}^{(1)},$$

$$h_{F,\,\text{loc}}^{(1)} = \frac{1}{2!\tau} \int_0^\tau \mathrm{d}t_1 \int_0^{t_1} \mathrm{d}t_2 \, \{H^S(t_1), H^S(t_2)\}, \qquad (42)$$

$$h_{F,\,\text{int}}^{(1)} = \frac{1}{2!\tau} \int_0^\tau \mathrm{d}t_1 \int_0^{t_1} \mathrm{d}t_2$$
$$\times (\{H^R, H^S(t_2)\} + \{H^S(t_1), H^R\}).$$
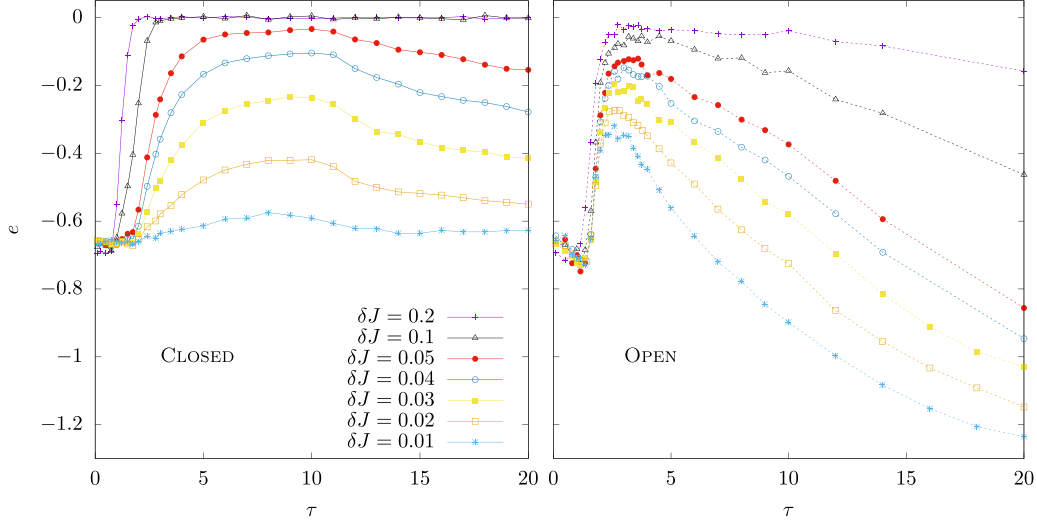
FIG. 6. Energy density of driven sites for a closed spin chain (left, $\ell = 40$) and an open one (right, $\ell = 20$, $L = 2000$). For the dynamical distributions, due to the symmetric structure of the Hamiltonian, energy density $e = 0$ corresponds to the "infinite-temperature" ensemble. In both plots, the strength of the disorder δJ increases from bottom to top, which leads to an increasingly steep rise in energy absorption around $\tau \approx 1$ in the closed system. The initial energy density has been chosen as $e_{\text{initial}} = -0.66$, and curves are averages over $\mathcal{N} = 8000$ trajectories at $t = 1000\tau$.

Here, $h_{F,\,\text{loc}}^{(1)}$ depends solely on degrees of freedom of the system proper. Furthermore, since only nearest-neighbor spins interact, $h_{F,\,\text{int}}^{(1)}$ depends only on the spins adjacent to the boundary of the system proper. By extension, since the Nth-order correction $\mathcal{H}_F^{(N)}$ involves N nested Poisson brackets, any modification of the reservoir Hamiltonian a distance M away from the system proper is suppressed by a factor of τ^M. As a result, the reservoir is only significantly affected by the driving in close vicinity to the system proper at sufficiently high frequencies. The small tails visible in Fig. 1 arise from such corrections. Consequently, we can expect net energy absorption to be small and a local picture to be sufficient for the description of the system proper in the high-frequency regime.

B. Low-frequency regime

1. Synchronization of the system proper

To understand the differences between the closed and the open systems in the low-frequency regime as exposed by Fig. 6, we may again invoke the rotating-frame picture of Sec. IV B. In the clean limit $\delta J \to 0$, the closed system is described by the effective Hamiltonian

$$H_{\text{rot}} = H_{\text{int}} + H_{\text{mag}} \quad \text{with}$$

$$H_{\text{int}} = -\sum_{j=1}^{\ell-1} \tilde{\mathbf{S}}_j \cdot \tilde{\mathbf{S}}_{j+1}, \tag{43}$$

$$H_{\text{mag}} = \sum_{j=1}^{\ell} (\hat{\mathbf{x}} - \omega\hat{\mathbf{z}}) \cdot \tilde{\mathbf{S}}_j.$$

As this Hamiltonian is time independent, one might *a priori* expect the system to relax to a Gibbs state with respect to H_{rot}. However, besides H_{rot}, H_{mag} is a conserved quantity, which is also a sum of local densities. As such, one would expect a

generalized Gibbs ensemble of the form [45]

$$P_{\text{G}} = \frac{1}{Z_{\text{G}}} \exp(-\lambda_{\text{int}} H_{\text{int}} - \lambda_{\text{mag}} H_{\text{mag}}), \tag{44}$$

where Z_{G} accounts for normalization, and the Lagrange multipliers λ_{int} and λ_{mag} are determined by the initial conditions. Since we sample from an isotropic initial state, we must have $\lambda_{\text{mag}} = 0$ so that also the ensemble (44) becomes isotropic; that is, its mean magnetization density vanishes. The mean magnetization density of the closed system is zero, and remains so in the laboratory frame. Reintroducing the disorder formally breaks all conservation laws and induces slow heating. However, since the rotational symmetry of the system is preserved on average, we can still expect that $\langle \mathbf{m} \rangle = 0$ on the relevant timescales. That is, the closed system does not synchronize with the drive. This expectation is indeed confirmed by our numerical results shown in Fig. 7, where residual oscillations can be attributed to the finite sample size and the disorder for details see Appendix A).

Once the reservoir is included, all local conservation laws of the system proper are broken and the full system is described by a rotating-frame Hamiltonian $\mathcal{H}_{\text{rot}}$ that features an inhomogeneous magnetic field [see Eq. (31)]. As a result, even for $\delta J \to 0$, there are no obvious conserved quantities other than $\mathcal{H}_{\text{rot}}$. The full system therefore relaxes to the global Gibbs state (32) on some long timescale, which we will further examine in the following section. On a much shorter timescale, the system proper attains the local Gibbs state (34), which, in contrast to the generalized Gibbs ensemble (44) is smoothly connected to the instantaneous equilibrium state of the adiabatic limit $\tau \to \infty$. It further gives rise to a finite mean magnetization in the rotating frame, which is responsible for the drop in the mean energy density of the system proper seen in Fig. 6. In the laboratory frame, the persistent magnetization of the system proper translates into a sinusoidally oscillating magnetization density, which may be
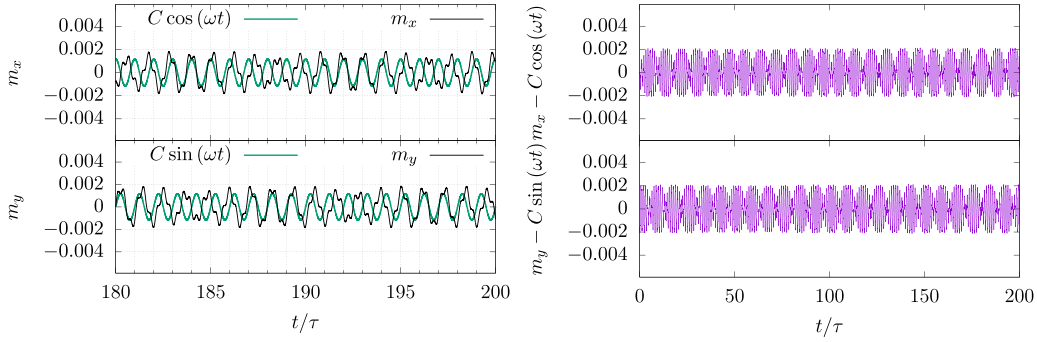
FIG. 7. Lack of synchronization of closed system. Left: Local magnetizations m_x and m_y, compared with the scaled magnetic field projected onto the appropriate direction, where the scaling factor $C = -0.00117$ has been fitted. Right: Difference between these functions. No synchronization is observable over any significant timescale. The observed oscillations result from the finite sample size and, to a lesser degree, the disorder (see Appendix A for details). Here, we have set $\tau = 10$, $\ell = L = 40$, $e_{\text{initial}} = -0.66$, and $\delta J = 10^{-3}$, and simulations are averaged over $\mathcal{N} = 4000$ trajectories.

observed in Fig. 8. Hence, the open system does synchronize with the drive up to small corrections, which are of the same order of magnitude as the remnant oscillations in the closed system and can likewise be traced back to disorder and finite sample size. Furthermore, for the parameters chosen in Fig. 8, the synchronized state is reached after about 100 cycles. For sufficiently weak disorder, this timescale is much shorter than that of the residual heating. However, since the local conservation laws of the system proper are broken only at its boundaries, we expect the synchronization time to grow with ℓ. More specifically, under the plausible assumption that the densities of magnetization and energy spread diffusively from the edge spins, the synchronization time would scale as ℓ^2.

2. Synchronization of the reservoir

Our understanding of the low-frequency regime rests on the assumption that in the rotating frame the system relaxes to the global Gibbs state of Eq. (32) on a timescale that is well separated from the heating timescale determined by δJ. Given the form of the z field present in the Hamiltonian of Eq. (31), one might expect that this relaxation happens uniformly throughout the reservoir. As a matter of causality, however, the reservoir spins far away from the driven sites

cannot be instantly affected by the driving. In fact, the interaction strength sets the scale for a finite group velocity $v \sim J = 1$, and any correlation function involving solely degrees of freedom separated by a distance r cannot distinguish between the driven and undriven systems outside of the light cone $r > vt$. Hence, the rearrangement of local degrees of freedom and the large-scale spread of correlations must occur on different timescales.

To uncover the inhomogeneous nature of the relaxation process explicitly, we calculate the spatial profiles of the local observables S_j^x and S_j^z. These data, plotted in Figs. 1 and 9, show that for low-frequency driving the x and z magnetizations of the system proper have settled to the flat profiles predicted by the local Gibbs state of Eq. (34) after around 1000 cycles. At this time, the z-magnetization profile of the reservoir is neither homogeneous nor stationary. To understand the mechanism of the subsequent global relaxation process, we may observe that the z magnetization is a locally conserved quantity everywhere in the bulk of the reservoir, up to corrections of order δJ. The breaking of this conservation law at the boundary of the reservoir, where the system proper generates an oscillating magnetic field perpendicular to $\hat{\mathbf{z}}$, leads to the buildup of a z-magnetization profile at strobo-scopic times, which spreads into the reservoir. In continuous
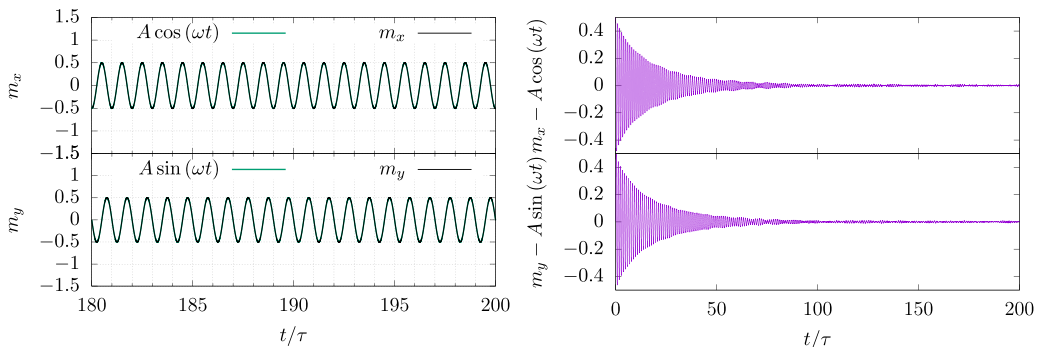
FIG. 8. Synchronization of open system. Left: Local magnetizations m_x and m_y, compared with the scaled magnetic field projected onto the corresponding direction, where the scaling factor $A = 0.501$ has been fitted. Right: Difference between these functions. There is a transient period of approximately 100 cycles, after which the system is well synchronized up to small errors, which result from disorder and finite sample size. Here, we have set $\tau = 10$, $\ell = 40$, $L = 2000$, $e_{\text{initial}} = -0.66$, and $\delta J = 10^{-3}$ and simulations are averaged over $\mathcal{N} = 800$ trajectories.
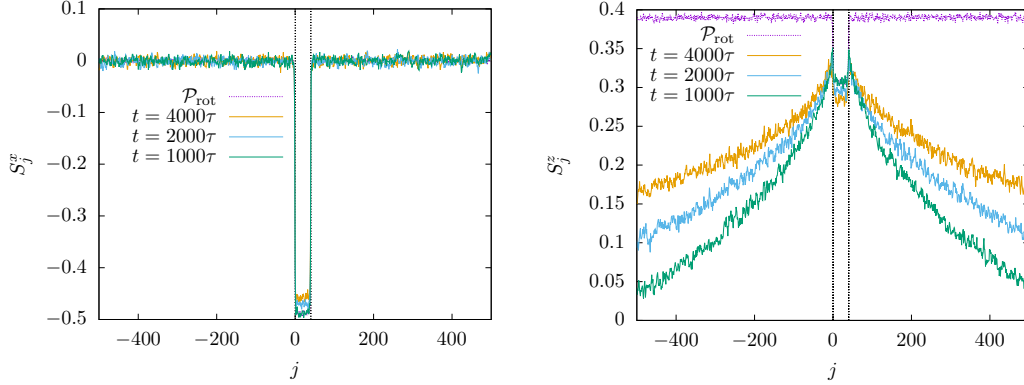
FIG. 9. Spatially resolved profiles for S_j^x and S_j^z in the slow-driving regime $\tau = 10$ for $\ell = 40$, $L = 2000$, $\delta J = 10^{-3}$, and $e_{\text{initial}} = -0.66$. Shown are the dynamical results, averaged over $\mathcal{N} = 8000$ trajectories, for various t, compared with the rotating-frame ensemble $\mathcal{P}_{\text{rot}}$ of Eq. (32) averaged over $\mathcal{M} = 32000$ MC samples. Boundaries of the system proper are indicated by vertical dashed lines.

time, this process corresponds to a gradual synchronization between the system proper and the reservoir. It continues until the full system has entirely relaxed to the global Gibbs state of Eq. (32) and the stroboscopic magnetization profile of the reservoir becomes flat. For $\delta J = 0$, the overall heating rate would then go to zero. Again, assuming a diffusive spreading of magnetization and energy densities would imply that the timescale until the full system has synchronized grows as L^2. For finite disorder, deviations from synchronization in the system proper cause small heat currents to flow into the reservoir and elevate its overall energy density on the heating timescale set by δJ. Notably, as we will see in the next section, the synchronization mechanism strongly suppresses overall energy absorption compared with local-dissipation models, which effectively force the reservoir to remain constantly in its original equilibrium state, that is, to act as a pure heat sink.

We may now return to the question of how to determine the effective inverse temperature β_{rot} for the rotating-frame ensemble encountered in Sec. IV B. According to statistical mechanics, this parameter should be fixed by energy conservation, as indicated by Eq. (33). However, this approach assumes that the system has fully relaxed to the global Gibbs state (32), which, as shown by Figs. 1 and 9, is clearly not the case for the evolution times considered in Fig. 5. It is therefore surprising that β_{rot} as determined by Eq. (33) yields excellent agreement between ensemble and dynamical distributions at very low frequencies [32]. *A posteriori*, this result may be attributed to the fact that the virtual magnetic field on the reservoir and, thus, the amplitude of the emerging magnetization profile are small for $\omega \ll 1$. Thus the initial state of the reservoir does not deviate substantially from its rotating-frame Gibbs state. Away from very low frequencies, agreement between ensemble and dynamical distributions may still be achieved by fitting β_{rot} to the mean energy of the system proper, as we have shown in Sec. IV B. This observation suggests that the reservoir locally reaches an effective equilibrium state at its boundary with the system proper on a much smaller timescale than that of the global relaxation process.

This reasoning implies an implicit relationship between the energy density of the system proper, e, and that of the entire system, $\mathfrak{e}$, which can be probed quantitatively. In the

rotating-frame ensemble (32), both e and $\mathfrak{e}$ are determined by a single parameter, β_{rot}. If we assume that relaxation to this ensemble occurs on a much faster timescale than heating, we may describe the system by an effective rotating-frame Gibbs state with inverse temperature $\beta_{\text{rot}} = \beta_{\text{rot}}(t)$ after some transient period. We may thus sweep β_{rot} through a range of values and plot the energy densities $\mathfrak{e}(\beta_{\text{rot}})$ against $e(\beta_{\text{rot}})$. This plot can then be compared with the actual values of these quantities obtained from dynamical simulations. The results of this analysis are shown in Fig. 10. For $\tau = 10$, the dynamical energy densities come fairly close to values predicted by the effective ensemble for simulation times $t \gtrsim 1000\tau$. In this regime, β_{rot} can be accurately determined from energy conservation, which yields excellent results as exhibited in Ref. [32]. For $\tau = 5$, Fig. 10 shows that this approach is viable only for $t \gtrsim 5000\tau$, which explains why β_{rot} required fitting in order to achieve agreement between dynamical and ensemble distributions as seen in Fig. 5 where $t = 1000\tau$.

C. Langevin model

Throughout this paper, we have explicitly modeled the reservoir and simulated its full microscopic dynamics. We have, however, not yet considered the option of accounting for the reservoir by modifying only the equations of the system proper, which might reduce the computational cost of numerical simulations. Arguably, the simplest way to construct the dissipative dynamics of the system proper is to replace the equations of motion for the edge spins with the Langevin equation [46–48]

$$\frac{d\mathbf{S}_j}{dt} = -\boldsymbol{\Omega}_j \times \mathbf{S}_j - \gamma_s \mathbf{S}_j \times (\mathbf{S}_j \times \boldsymbol{\Omega}_j)$$
$$+ \mathbf{h}_j(t) \times \mathbf{S}_j, \quad j = 1, \ell, \quad (45)$$

and for the remaining sites $j = 2, \ldots, \ell - 1$ the equations of motion [Eqs. (3)] remain unchanged. Here, $\mathbf{h}_j(t)$ represents a δ-correlated noise vector $\langle h_{i,\alpha}(t)h_{j,\beta}(t') \rangle = \mu_s \delta_{ij}\delta_{\alpha\beta}\delta(t - t')$, μ_s is the noise strength, and γ_s is a damping constant. To mimic a thermal reservoir at inverse temperature β, these quantities must obey the fluctuation-dissipation relation $2\gamma_s = \mu_s\beta$.
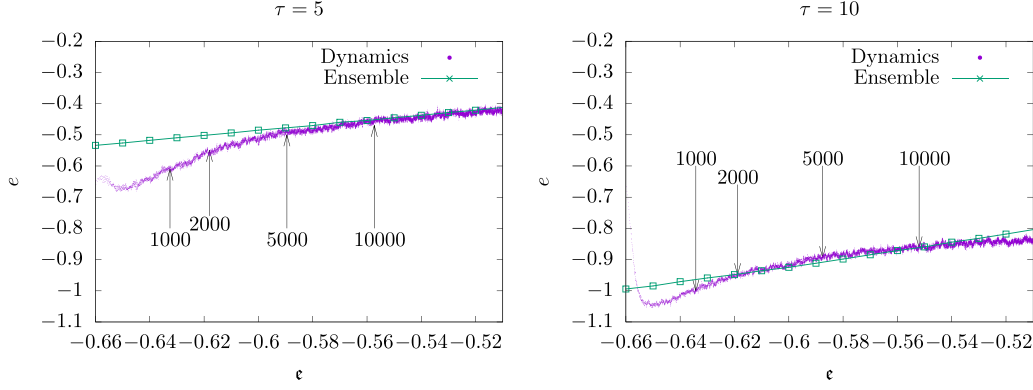
FIG. 10. Implicit relationship between the energy density of the total system, ε, and the system proper only, e. The green curve is produced by sweeping β_{rot} and evaluating the energy density of both system proper and total system from the ensemble of Eq. (32). The purple data points are an average of $\mathcal{N} = 8000$ dynamical evolutions with $\ell = 40$, $L = 4000$, $\delta J = 10^{-3}$, and $e_{\text{initial}} = -0.66$. The number of cycles elapsed is indicated by arrows.

If the effective magnetic field $\boldsymbol{\Omega}_j$ is time independent, the system proper would relax to the Gibbs state (4) under the dissipative dynamics generated by Eq. (45). One might now include the driving by adding the on-site magnetic field $\mathbf{B}(t)$ to the effective field $\boldsymbol{\Omega}_j$. However, given our results so far, we expect that this modification will invalidate the basic assumptions underpinning Langevin equation (45). Specifically, the Markovian limit, i.e., δ-correlated noise, is realized only if the reservoir constantly remains in its initial equilibrium state and its correlation functions decay fast on the observational timescale. As seen in Figs. 1 and 9, however, the full dynamical simulation suggests that, even for $L \to \infty$, an ever-growing region of the reservoir departs from its initial state while correlations with the system proper build up continuously. One should therefore not expect a simple Langevin model with additively incorporated driving to reproduce the dynamics of the system proper accurately, at least beyond the limit of ultralow frequencies, which is characterized by relaxation to an instantaneous Gibbs state.

To corroborate this expectation, we simulate the Langevin model defined by Eqs. (3) and (45) for the bulk and the boundaries of the system proper, respectively; that is, the driving is incorporated by adding $\mathbf{B}(t)$ to $\boldsymbol{\Omega}_j$ as described above. To this end, we follow the numerical approach of Ref. [46], which still relies on the alternated updating algorithm described in Sec. II B. The Suzuki-Trotter decomposition of the time-evolution operator is now given by

$$U(t + \delta t, t) = e^{\frac{\delta t}{2} \mathcal{L}_{t+\delta t/2}^D} e^{\frac{\delta t}{2} \mathcal{L}_{t+\delta t/2}^A} e^{\delta t \mathcal{L}_{t+\delta t/2}^B}$$
$$\times e^{\frac{\delta t}{2} \mathcal{L}_{t+\delta t/2}^A} e^{\frac{\delta t}{2} \mathcal{L}_{t+\delta t/2}^D} + \mathcal{O}(\delta t^3), \quad (46)$$

where the operator $\mathcal{L}_{t+\delta t/2}^D$ describes the damping acting on the boundary spins, i.e., the term proportional to γ_s in Eq. (45). The stochastic magnetic fields are obtained from the formula $h_{i,\alpha}(t) = \eta \sqrt{\mu_s/\delta t}$, where η is a random variable that is independently sampled from a standard normal distribution $\mathcal{N}(0, 1)$ for every field component $i = x, y, z$, every boundary spin $\alpha = 1, \ell$, and every time step δt. The stochastic fields are then added to the systematic fields $\boldsymbol{\Omega}_1$ and $\boldsymbol{\Omega}_\ell$, which enter the Liouville operators $\mathcal{L}_{t+\delta t/2}^{A|B}$. Note that the damping operator $\mathcal{L}_{t+\delta t/2}^D$ does not directly depend on the stochastic fields.

Using the method described above, we calculate the mean energy density of the driven system proper as a function of the driving period τ and the exposure time t, where the system is initially prepared in a Gibbs state with respect to the inverse temperature β and the free Hamiltonian $H_0 = -\sum_{j=1}^{\ell-1} \mathbf{S}_j^{\mathsf{T}} J_j \mathbf{S}_{j+1}$. The results of this analysis, which are shown in the first row of Fig. 11, reveal clear qualitative differences between the Langevin model and the Hamiltonian model that we have considered before. First, the high-frequency regime, which is characterized by a strong suppression of energy absorption for $\tau \lesssim 2$ in the Hamiltonian model, is not reproduced by the Langevin model at all; instead the system proper seems to relax to a stroboscopic steady state, which continuously approaches its instantaneous Gibbs state as τ increases. Second, while in both models the mean energy density of the system proper drops below its initial value at low frequencies, which indicates synchronization between the drive and the system proper, disorder-induced heating persists for $\tau \gtrsim 2$ in the Hamiltonian model. By contrast, the stroboscopic energy density of the system proper becomes time independent in the Langevin model at sufficiently long times. Notably, these observations persist even when the damping constant γ_s, which is the only parameter of the Langevin model that does not have a direct correspondent in the Hamiltonian model, is of the same order of magnitude as the disorder strength δJ. However, we note that one would naturally expect γ_s to be of the same order of magnitude as the interaction strength between neighboring spins which determines the rate of energy exchange between the system proper and the reservoir. Following this argument, we should set $\gamma_s \simeq 1$ for a fair comparison.

For an even more striking comparison, we now consider the total energy absorption $\Delta E(t)$. For the Hamiltonian model, this quantity can be found directly from the Hamiltonian of the full system $\mathcal{H}(t)$ as

$$\Delta E(t) = \mathcal{H}(0) - \mathcal{H}(t). \quad (47)$$

In the Langevin model, $\Delta E(t)$ can be determined by integrating the rate of energy absorption,
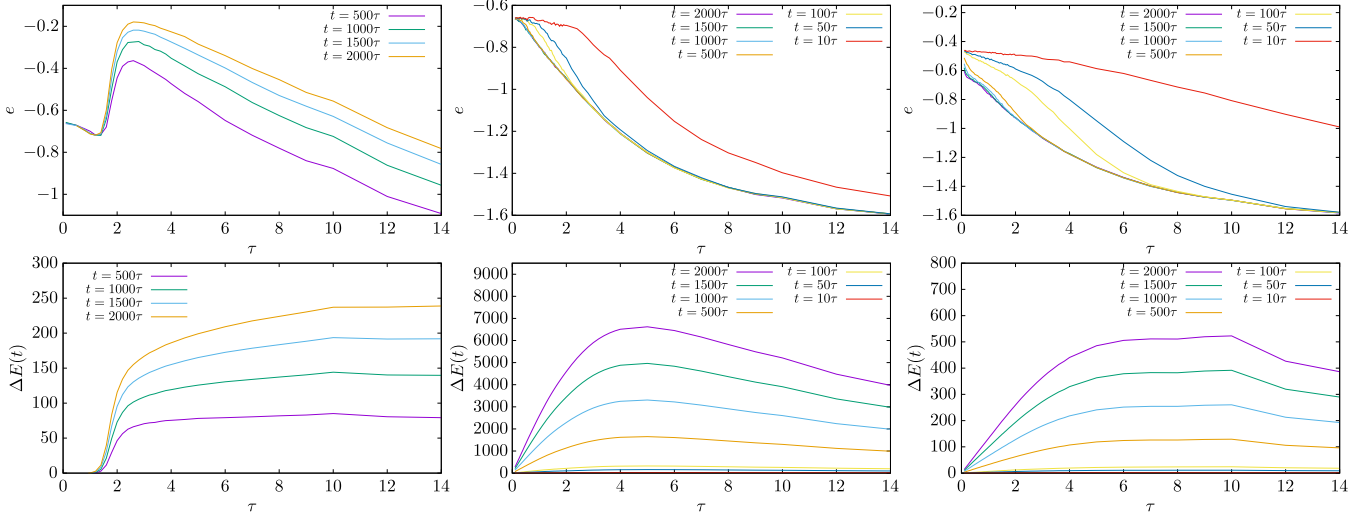
FIG. 11. Hamiltonian vs Langevin model. First row: Mean energy density of the system proper as a function of the driving period τ for different values of the exposure time t. Second row: Total energy absorption as a function of τ for different values of t. The first column corresponds to the Hamiltonian model with $\ell = 20$, $L = 2000$, and $e_{\text{initial}} = -0.66$. The plots in the second column were obtained for a Langevin model with $\ell = 20$ and $\beta = 2.888$, which corresponds to the equilibrium energy density $e_{\text{eq}} = -0.66$. The damping constant cannot be directly inferred by comparison with the Hamiltonian model. However, it is plausible to assume that this parameter should be of the same order of magnitude as the strength of the interaction between adjacent spins. Therefore, we have set $\gamma_s = 1$ in the second column. For completeness, we show in the third column the same plots as in the second one for $\gamma_s = 5 \times 10^{-2}$, i.e., a value of the damping constant that is comparable with the disorder strength. For all plots, we have set $\delta J = 2 \times 10^{-2}$ and averaged over $N = 8000$ trajectories corresponding to different initial conditions and realizations of the disorder and the noise.

that is,

$$\Delta E(t) = \int_0^t ds \left\langle \frac{d}{ds} H(s) \right\rangle_0 = \ell \int_0^t ds \, \dot{\mathbf{B}}(s) \cdot \langle \mathbf{m} \rangle_0$$

$$= \ell \omega \int_0^t ds \, [\langle m_y \rangle_0 \cos(\omega s) - \langle m_x \rangle_0 \sin(\omega s)], \quad (48)$$

where $\langle \cdots \rangle_0$ indicates the average over initial states and realizations of the disorder and the noise. The corresponding results are plotted in the second row of Fig. 11. Besides the absence of the high-frequency plateau in the Langevin model, we find that the total energy absorption is increased by one order of magnitude for $\gamma_s = 1$ and still by a factor of 2 for $\gamma_s = 5 \times 10^{-2}$ compared with the Hamiltonian model. This observation confirms that the synchronization between system proper and reservoir, which, as discussed in Sec. V B 2, is indicated by a gradual buildup of a magnetization profile on the reservoir in the Hamiltonian model, and cannot be reproduced in the Langevin model, where the reservoir is assumed to be constantly in thermal equilibrium, does indeed substantially suppress the absorption of energy from the drive.

VI. PERSPECTIVES

The central aim of this paper was to shed light on the physics of classical many-body systems that are subject to periodic driving while being coupled to a large reservoir. To make progress in this direction, we have modeled both the driven system and the reservoir as spin chains with nearest-neighbor interactions and weak disorder. Since the full Hamiltonian dynamics of this setup can be simulated exactly at moderate numerical cost, we were able to avoid the use of

dissipative equations of motion that account for the reservoir in a phenomenological or approximate way. While some of our more quantitative results may be contingent on the specific setting we have considered, we expect our main insights to be representative for a broader class of systems. In particular, a high-frequency regime, where energy absorption is strongly suppressed and the stroboscopic dynamics of the driven system is governed by its averaged Hamiltonian, plus leading corrections obtained from the classical Floquet-Magnus expansion, should generically exist. Our results corroborate the natural expectation that, in this regime, the reservoir acts, up to small perturbations at its boundary with the driven system, as a nearly-reversible heat sink balancing residual energy uptake from the drive.

Perhaps more surprisingly, we found that this behavior changes quite abruptly as the driving frequency decreases below some threshold value, which is determined by the typical energy scale of the system and, to a lesser degree, by the strength of the disorder (see Fig. 6). The system then enters a crossover regime, which is characterized by a sharp increase in energy absorption and covers only a small range of frequencies. Understanding the microscopic mechanism of this crossover as well as its putative dependence on the dimensionality of the system, the nature of the drive, and the range of interactions, provides an intriguing and presumably challenging subject for future research.

Upon further reducing the driving frequency, the system eventually enters a low-frequency regime, which connects smoothly to the, most likely universal, quasistatic limit, where the driven degrees of freedom are constantly described by an instantaneous equilibrium state. This regime is characterized by rapid synchronization between the driven system and the

applied field. Away from the quasistatic limit, a continuous rearrangement of reservoir degrees of freedom over long distances takes place. This process is accompanied by the steady buildup of long-range correlations and the gradual synchronization between the driven system and the reservoir. Here, we were able to show that this behavior may in fact extend over a large range of frequencies, which is limited from above only by the crossover to the high-frequency regime. This analysis, however, crucially relies on the existence of a rotating reference frame, where the Hamiltonian of the entire system is nearly time independent, thus providing a stroboscopically conserved quantity. Whether or not almost conserved quantities, which prevent the system from approaching an infinite-temperature state on a practically long timescale, exist for more general systems and driving protocols remains an open question. It is, however, plausible to expect that such quantities may be constructed at least perturbatively from the quasistatic limit, where the instantaneous Hamiltonian serves as an adiabatic invariant. It would then be interesting to explore whether a qualitatively new type of behavior emerges between the low-frequency regime and the crossover to the high-frequency regime and how it can be characterized.

Finally, our work opens an interesting prospect in the area of open dynamical systems out of equilibrium. As we have shown in Sec. V, the established Langevin approach to classical open-system dynamics fails to reproduce the behavior of the driven system that we observe in our first-principles simulations. In a wider perspective, our results show that any attempt to describe the dynamics of the system proper at intermediate frequencies by means of dissipative equations of motion would have to give up on the condition of Markovianity, which rests on the assumption of a nearly invariant reservoir with fast-decaying correlations on the observational timescales. For the system we have analyzed here, this condition can be met only near the quasistatic limit, and perhaps in the high-frequency regime upon replacing the system Hamiltonian with a suitably truncated Floquet-Magnus Hamiltonian; in the latter case, it may be possible to develop a classical framework similar to the stochastic-wave-function method in Floquet representation, which provides a dynamical description for open quantum systems subject to rapidly oscillating driving fields [49]. For intermediate frequencies, however, our results strongly suggest that non-Markovian equations of motion will have to be adopted to describe the dynamics of periodically driven open systems, presumably in both the classical and the quantum case. Understanding whether it is indeed possible to derive such time-evolution equations, e.g., by using Nakajima-Zwanzig projection-operator techniques [50–52], and whether they can be cast into a practically tractable form will require further research. Our present work provides both a well-defined starting point for such investigations and a valuable benchmark for their results.

The source code used for all simulations, and all data used in figures, is freely available [53].

ACKNOWLEDGMENTS
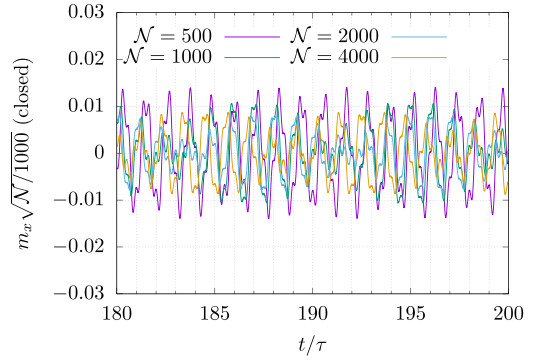
FIG. 12. Local magnetization density m_x of the closed system as a function of time and rescaled with $\sqrt{\mathcal{N}}$ for different sample sizes $\mathcal{N}$. The remaining parameters are the same as in Fig. 7. As all curves show similar overall amplitudes, this plot confirms that oscillations are suppressed with $\sqrt{\mathcal{N}}$ as is required by the central limit theorem (see also Appendix B). The beating frequency ω_- of the magnetization vector in the clean system, where $\delta J = 0$, is still visible in the weakly disordered system upon noting that $2\pi/\omega_- \simeq 11$ for $\tau = 2\pi/\omega = 10$. We have set $L = 20$, $\ell = 20$, $\delta J = 10^{-3}$, $\mathfrak{e}_{\text{initial}} = -0.66$, and $\tau = 10$.

APPENDIX A: CLOSED SYSTEM REVISITED

We consider the closed system as discussed in Sec. V A. For $\delta J = 0$, the magnetization vector $\mathbf{M} = \sum_{j=1}^{\ell} \mathbf{S}_j$ behaves like a single spin and follows the equation of motion

$$\frac{d}{dt}\mathbf{M} = \mathbf{B}(t) \times \mathbf{M}. \tag{A1}$$

For $\mathbf{B}(t) = (\cos(\omega t), \sin(\omega t), 0)^{\mathsf{T}}$, this differential equation can be solved exactly and yields a solution of the form $\mathbf{M}(t) = V(t)\mathbf{M}(0)$, where the matrix $V(t)$ is a quasiperiodic function of time with frequencies ω and $\omega_\pm = \sqrt{1 + \omega^2} \pm \omega$. Thus, the mean magnetization density at the time t is given by $\mathbf{m}(t) = \frac{1}{\ell}V(t)\langle\mathbf{M}(0)\rangle_0 = 0$, where the average of $\mathbf{M}(0)$ vanishes since we sample initial states from an isotropic ensemble. This result shows that, for sufficiently small δJ, remnant oscillations of the magnetization density of the closed system on observable timescales are an artifact of finite sample sizes, as we demonstrate explicitly in Fig. 12.

APPENDIX B: ERROR ANALYSIS

The results presented in this paper rely on numerical simulations and therefore on averages over necessarily finite samples. To understand the error introduced by finite sampling quantitatively, we here consider the energy density of the system proper as a representative example. This quantity is obtained as follows. We first sample a particular realization of the disorder from the normal distribution $\mathcal{N}(1, \delta J)$ and

an initial $\{\mathbf{S}_j(0)\}$ state of the full system from the thermal ensemble (4) for given inverse temperature β and system sizes ℓ and L. The initial state is then evolved for a given time t with a fixed period τ of the oscillating magnetic field acting on the system proper. This simulation yields a single sample for the energy density at the time t,

$$\hat{e}_k = e(\{\mathbf{S}_j(t)\}), \tag{B1}$$

where $\{\mathbf{S}_j(t)\}$ is the evolved state of the full system. Upon repeating this procedure $\mathcal{N}$ times, we obtain the average

$$e(\mathcal{N}) = \frac{1}{\mathcal{N}} \sum_{k=1}^{\mathcal{N}} \hat{e}_k. \tag{B2}$$

At the same time, we can calculate the approximate variance of the distribution of the energy density,

$$\sigma_e^2(\mathcal{N}) = \frac{1}{\mathcal{N}} \sum_{k=1}^{\mathcal{N}} \hat{e}_k^2 - e^2(\mathcal{N}). \tag{B3}$$

This quantity represents the width of the probability distribution around the mean, and is not a measure of the deviation of the finite sum (B2) from its limit for $\mathcal{N} \to \infty$. An estimate for the statistical error of the mean itself is obtained by considering that, for any fixed set of parameters, the $\hat{e}_k$
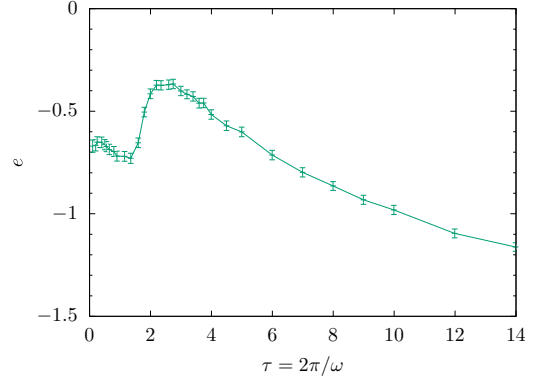
FIG. 13. Energy density of the system proper after 1000 driving cycles for $L = 2000$, $\ell = 20$, and $\delta J = 10^{-3}$. Here we have averaged over $\mathcal{N} = 1000$ trajectories. The error bars have a width of $\hat{\sigma}_e(\mathcal{N})/\sqrt{N}$ and show that errors due to finite sampling are not qualitatively significant.

represent independent and identically distributed random variables. Thus, by the central limit theorem, the sum in Eq. (B2) corresponds to the mean value of a normal distribution with variance $\hat{\sigma}_e^2 = \sigma_e^2/\mathcal{N}$, where $\hat{\sigma}_e^2 = \lim_{\mathcal{N} \to \infty} \hat{\sigma}_e^2(\mathcal{N})$. For sufficiently large $\mathcal{N}$, the error may be estimated by $\hat{\sigma}_e(\mathcal{N})/\sqrt{\mathcal{N}}$. This quantity is shown in Fig. 13.

[1] G. Floquet, Ann. Sci. Ec. Norm. Super. **12**, 47 (1883).

[2] T. Kitagawa, T. Oka, A. Brataas, L. Fu, and E. Demler, Phys. Rev. B **84**, 235108 (2011).

[3] H. Sambe, Phys. Rev. A **7**, 2203 (1973).

[4] M. Torres and A. Kunold, Phys. Rev. B **71**, 115313 (2005).

[5] M. Bukov, L. D'Alessio, and A. Polkovnikov, Adv. Phys. **64**, 139 (2015).

[6] A. Eckardt, Rev. Mod. Phys. **89**, 011004 (2017).

[7] We thank Anatoli Polkovnikov for bringing this argument to our attention.

[8] V. I Arnold and A. Avez, *Ergodic Problems of Classical Mechanics* (W. A. Benjamin, Inc., New York, 1968).

[9] H. W. Broer and B. Krauskopf, AIP Conf. Proc. **548**, 31 (2000).

[10] L. D. Landau and E. M. Lifshitz, *Mechanics* (Pergamon Press, New York, 1960), Vol. 1, Sec. 30.

[11] T. Kinoshita, T. Wenger, and D. S. Weiss, Nature (London) **440**, 900 (2006).

[12] V. Khemani, A. Lazarides, R. Moessner, and S. L. Sondhi, Phys. Rev. Lett. **116**, 250401 (2016).

[13] C. W. von Keyserlingk and S. L. Sondhi, Phys. Rev. B **93**, 245145 (2016).

[14] A. Chan, A. De Luca, and J. T. Chalker, Phys. Rev. X **8**, 041019 (2018).

[15] C. Weitenberg and J. Simonet, Nat. Phys. **17**, 1342 (2021).

[16] M. S. Rudner and N. H. Lindner, Nat. Rev. Phys. **2**, 229 (2020).

[17] P. Ponte, A. Chandran, Z. Papic, and D. A. Abanin, Ann. Phys. **353**, 196 (2015).

[18] A. Lazarides, A. Das, and R. Moessner, Phys. Rev. E **90**, 012110 (2014).

[19] A. Russomanno, A. Silva, and G. E. Santoro, J. Stat. Mech. (2013) P09012.

[20] T. N. Ikeda and A. Polkovnikov, Phys. Rev. B **104**, 134308 (2021).

[21] A. Haldar and A. Das, J. Phys.: Condens. Matter **34**, 234001 (2022).

[22] A. Lazarides, A. Das, and R. Moessner, Phys. Rev. Lett. **112**, 150401 (2014).

[23] D. Abanin, W. De Roeck, W. W. Ho, and F. Huveneers, Commun. Math. Phys. **354**, 809 (2017).

[24] D. A. Abanin, W. De Roeck, W. W. Ho, and F. Huveneers, Phys. Rev. B **95**, 014112 (2017).

[25] D. A. Abanin, W. De Roeck, and F. Huveneers, Phys. Rev. Lett. **115**, 256803 (2015).

[26] T. Mori, T. Kuwahara, and K. Saito, Phys. Rev. Lett. **116**, 120401 (2016).

[27] T. Kuwahara, T. Mori, and K. Saito, Ann. Phys. **367**, 96 (2016).

[28] W. Hodson and C. Jarzynski, Phys. Rev. Res. **3**, 013219 (2021).

[29] O. Howell, P. Weinberg, D. Sels, A. Polkovnikov, and M. Bukov, Phys. Rev. Lett. **122**, 010602 (2019).

[30] A. Pizzi, A. Nunnenkamp, and J. Knolle, Phys. Rev. Lett. **127**, 140602 (2021).

[31] A. J. McRoberts, T. Bilitewski, M. Haque, and R. Moessner, Phys. Rev. B **105**, L100403 (2022).

[32] T. Veness and K. Brandner, preceding paper, Phys. Rev. E **108**, L042102 (2023).

[33] In the $\delta J = 0$, $\mathbf{B} = 0$ case, there are three conserved quantities in addition to the Hamiltonian, namely, each component of the total magnetization: M_x, M_y, and M_z. Later discussions of conservation laws are to be understood for more general systems where there may be more, and nonetheless the general phenomenology may remain unchanged.

[34] F. Jin, T. Neuhaus, K. Michielsen, S. Miyashita, M. A. Novotny, M. I. Katsnelson, and H. De Raedt, New J. Phys. **15**, 033009 (2013).

[35] M. Krech, A. Bunker, and D. P. Landau, Comput. Phys. Commun. **111**, 1 (1998).

[36] M. E. J. Newman and G. T. Barkema, *Monte Carlo Methods in Statistical Physics* (Clarendon Press, Oxford, UK, 1999).

[37] J. D. Parsons, Phys. Rev. B **16**, 2311 (1977).

[38] A. Erdélyi, *Asymptotic Expansions* (Dover, New York, 1956).

[39] S. Blanes, F. Casas, J. A. Oteo, and J. Ros, Phys. Rep. **470**, 151 (2009).

[40] C. M. Bender and S. Orszag, *Advanced Mathematical Methods for Scientists and Engineers I: Asymptotic Methods and Perturbation Theory* (McGraw-Hill, New York, 1999), Vol. 1.

[41] M. Berry, *Asymptotics Beyond All Orders* (Springer, Boston, 1991).

[42] T. Mori, Phys. Rev. B **98**, 104303 (2018).

[43] E. B. Fel'dman, Phys. Lett. A **104**, 479 (1984).

[44] A. Rubio-Abadal, M. Ippoliti, S. Hollerith, D. Wei, J. Rui, S. L. Sondhi, V. Khemani, C. Gross, and I. Bloch, Phys. Rev. X **10**, 021044 (2020).

[45] A. Polkovnikov, K. Sengupta, A. Silva, and M. Vengalattore, Rev. Mod. Phys. **83**, 863 (2011).

[46] P. W. Ma and S. L. Dudarev, Phys. Rev. B **83**, 134418 (2011).

[47] P. W. Ma, S. L. Dudarev, A. A. Semenov, and C. H. Woo, Phys. Rev. E **82**, 031111 (2010).

[48] W. F. Brown, Phys. Rev. **130**, 1677 (1963).

[49] H.-P. Breuer and F. Petruccione, Phys. Rev. A **55**, 3101 (1997).

[50] S. Nakajima, Prog. Theor. Phys. **20**, 948 (1958).

[51] R. Zwanzig, J. Chem. Phys. **33**, 1338 (1960).

[52] H.-P. Breuer and F. Petruccione, *Theory of Open Quantum Systems* (Oxford University Press, Oxford, UK, 2002).

[53] https://github.com/tveness/spinchain-papers